Chapter 16
Parametric Blending and FE-Optimisation of a Compressor Blisk Test Case

Kai Karger and Dieter Bestle

Abstract Due to raising demands from aviation industry concerning weight reduction and increased efficiency, compressor front stages of jet engines are designed as blade integrated disks (blisks). However, a major drawback of blisks is that small cracks from foreign object impacts occurring in service may propagate into the whole disk causing burst at worst case which is unacceptable. As a damaged blade of a blisk cannot easily be replaced, there is a need for repair. For example, borescope blisk blending may be applied on-wing to ensure safe on-going operation. To determine best solutions for the blending shape, process integration and optimisation tools are used which modify a parametric model and examine its impact on fatigue criteria by FEM.

Keywords Blisk · Blending · FEM · Process integration · Optimisation

16.1 Introduction

Actually, modern civil jet engines are developed towards higher efficiency and lower weight. Especially at the front stages of compressors, blade integrated disks (blisks) may contribute to both demands since they have less leakage flow and lower weight than bladed disks. However, such blisks are characterised by low vibration damping and they need a higher foreign object damage resistance to ensure rotor integrity. Therefore, stricter design criteria for vibration resistance and static stresses are required. Further, single blades cannot be replaced easily in case of damage demanding repair strategies such as blending which is investigated in this paper within an industrial test case. A fictional elliptical dent at the leading edge of an

K. Karger · D. Bestle (✉)
Chair of Engineering Mechanics and Vehicle Dynamics, Brandenburg University of Technology, P.O.BOX 101344, 03013 Cottbus, Germany
e-mail: bestle@tu-cottbus.de

K. Karger
e-mail: kai.karger@tu-cottbus.de

D. Greiner et al. (eds.), *Advances in Evolutionary and Deterministic Methods for Design, Optimization and Control in Engineering and Sciences*, Computational Methods in Applied Sciences 36, DOI 10.1007/978-3-319-11541-2_16

aerofoil is used to represent the damage causing a strong decay of the fatigue criteria below demanded lower bounds. By smoothly cutting out the damaged area, the fatigue criteria shall be recovered to original conditions.

Existing guidelines for borescope blending repair use circular scallops to be applied perpendicularly to the blades if a damage occurs at the mid height area [6]. Rules for geometric limits have been determined within aerodynamic investigations [5, 12] where the strongest limitation is that the fillet region must not be blended. In order to provide fast results for maintenance, typically the creation of a database for standard blending procedures is suggested [3].

The scope of this work is to find optimal blending shapes for a given damage by an automated optimisation process where a parametric blending shape is modified, relevant endurance measures for a blisk are evaluated by FEM, and optimisation objectives and constraint criteria are computed. To speed up optimisation, Kriging-based surrogate models are used which allow to use genetic algorithms.

16.2 Parametric Model and Evaluation Process

Borescope blending is an in-situ-abrade procedure to repair aerofoils suffering from small foreign object damages. This can be done during regular visual engine inspections using borescopes without time-consuming disassembly of the engine and by supervising the repair process with cameras. Due to space limitations simple cutout geometries are realised on-wing. A flexible motor driven shaft is inserted through borescope ports. At the end of the shaft diverse tool kits can be mounted for nick, dent or crack removal. They are then positioned for blend repair according to engine manufacturer guidelines. In this paper, the resulting contour for damage removal is chosen as a D-shape (Fig. 16.1), where a tool with radius R starts at an adjustment height A with an attack angle α, permeates the aerofoil with depth D and ends at height H. These blending shape parameters may be summarised in the design vector

$$\mathbf{p} = [D\ A\ H\ R\ \alpha]^T \tag{16.1}$$

to be determined by an optimisation process.

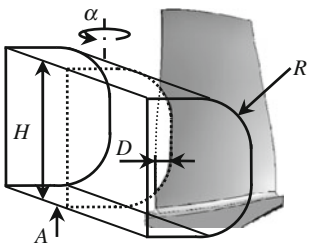

Fig. 16.1 Parametric blending shape model

A major goal of the repair process is to ensure structural feasibility. Here, fatigue criteria [10, 11] for regular conditions are used as constraints where the maximum stresses $\sigma_{\max}$ of the blade must not exceed the yield stress R_m, i.e.,

$$\sigma_{\max} \leq R_m, \tag{16.2}$$

to prevent it from plastic deformation. Another endurance measure is flutter stability. Flow excited vibrations of the blades can be avoided most likely if the ratio λ of natural blade frequency $2\pi f$ and flow excitation frequency $v_{rel,75\,\%}/c_{75\,\%}$is above a mode dependent lower bound λ^c found from experimental tests [11]:

$$\lambda_j := \frac{2\pi f_j \cdot c_{75\,\%}}{v_{rel,75\,\%}} \geq \lambda_j^c, \quad j \in \{1\mathrm{F}, 1\mathrm{T}\}. \tag{16.3}$$

Especially critical are the first flap (1F) and the first torsion (1T) mode resulting in constraints $\lambda_{1\mathrm{F}} \geq \lambda_{1\mathrm{F}}^c, \lambda_{1\mathrm{T}} \geq \lambda_{1\mathrm{T}}^c$. Equation (16.3) considers the relative flow velocity $v_{rel,75\,\%}$ and the chord length $c_{75\,\%}$ at 75 % radial blade height.

Besides static stresses, also dynamic stresses due to vibration must be taken into account. The *af*-strength is a combination of static and dynamic stresses according to the Goodman-diagram regarding fatigue stress R_f, dynamic stresses σ_{dyn}, static stresses σ_{stat}, and yield stress R_m, which has to be kept above an experience based level af^c:

$$af_j := \frac{R_f}{\sigma_{j,\mathrm{dyn}}} \left(1 - \frac{\sigma_{j,\mathrm{stat}}}{R_m}\right) \geq af_j^c, \quad j \in \{1\mathrm{F}, 1\mathrm{T}, 1 \ldots 4\}. \tag{16.4}$$

Again, first flap and first torsion modes are identified as critical using specific lower bounds $af_{1\mathrm{F}}^c, af_{1\mathrm{T}}^c$, whereas four other modes use a common lower bound $af_1^c = \cdots = af_4^c := af^c$.

In addition to the regular load case, also gas loads of a numerical surge event representing worst case running conditions are taken into account. Here, maximum stresses during surge should not exceed yield stress R_m:

$$\sigma_{\max}^{\mathrm{surge}} \leq R_m. \tag{16.5}$$

Flutter stability and *af*-strength from Eq. (16.3) respectively Eq. (16.4) are not used as constraints for numerical surge conditions, since surge events happen for a short period of time only. Both values define endurance levels and it is not intended to run an engine permanently at surge.

In order to get the necessary information on constraint functions (16.2)–(16.5) for specific design values (16.1), the blended rotor blisk is evaluated by the commercial FE-software ANSYS 13.0 [1]. Typically, aerofoil shapes are defined at running conditions, and a hot-to-cold transformation is required to determine the unloaded aerofoil shape before blending can be performed and various loads can be applied. This cold manufacturing geometry needs to be computed only once and was delivered by an

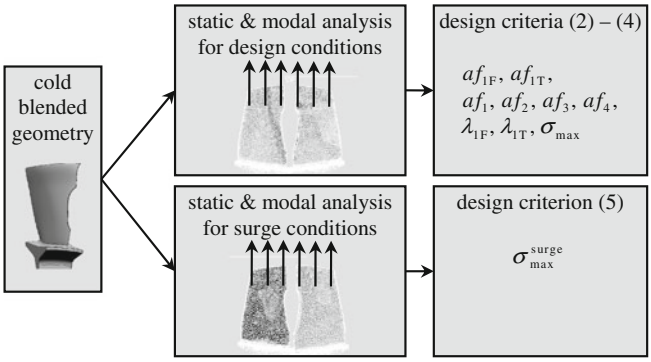

Fig. 16.2 Process flow for FE blisk evaluation

industrial partner. The cold blended blisk model is then used as input for non-linear static analyses and subsequent pre-stressed modal analyses to deliver relevant fatigue criteria [8]. The second step is an FE-analysis for surge conditions resulting in a different stress distribution, and hence changed fatigue criteria. A rough scheme of this FE-evaluation process is shown in Fig. 16.2.

In order to get some reference results, the FE-evaluation is firstly carried out for the undamaged and the damaged rotor blisk, respectively. The damaged blade is simulated by an elliptical damage of depth 2 mm and height 1 mm at 25 % radial blade height. For the damaged blade many of the endurance measures decay below the undamaged values, see Fig. 16.3 which shows normalised endurance measures $\overline{af}_j := af_j/af_j^c$, $\bar{\lambda}_{1F} := \lambda_{1F}/\lambda_{1F}^c$, $\bar{\lambda}_{1T} := \lambda_{1T}/\lambda_{1T}^c$, $\bar{\sigma}_{max} := R_m/\sigma_{max}$, and $\bar{\sigma}_{max}^{surge} := R_m/\sigma_{max}^{surge}$. Especially the maximum stress for surge loads is highly increased which would lead to serious blade damage. Obviously also the required values of *af*-strength for lower modes $af_{1F}, af_{1T}, af_1, af_2$ cannot be fulfilled by the damaged blade anymore, whereas the values of flutter stability $\lambda_{1F}, \lambda_{1T}$ and *af*-strengths af_3, af_4 change only slightly and still meet the required limits. The question arises if proper blending can bring up the violated criterion values above the necessary level.

16.3 Optimisation Problem and Automated Design Approach

In order to find a proper repair geometry, different blending shapes have to be created and evaluated within an optimisation process where each iteration step involves several subtasks to be coupled. Such a process integration may be done e.g. within the software package Isight 4.0 [2] which eases automation of computational tasks. Each design evaluation starts with a modification of the blending shape parameters (16.1) in an expression file which acts as input to the CAD programme Unigraphics NX 6.0. The CAD programme is used to adapt the model geometry and to determine

the blade mass. The blended geometry is then updated in a template of the FE-model and analysed with ANSYS 13.0. Based on the results, the objective and constraint values are written to files which are then parsed to the optimisation algorithm which suggests a new design vector for the next loop. In the following, an overview on the design objectives and the implemented optimisation strategy is given.

To ensure minimal impact on aerodynamic performance and minimal rotor imbalance, the blending volume should be as small as possible. However, structural feasibility has to be met as well. Regarding fatigue criteria, a bigger cutout leads to lower blade mass and greater notch radii which may result in lower stresses and better fatigue criteria. In order to meet both design goals, two conflicting targets are defined. For keeping the cutout size low, the ratio between undamaged blade mass m^{ref} and blade mass after blending m^{blend} is minimised:

$$f_1 = \frac{m^{\text{ref}}}{m^{\text{blend}}}. \tag{16.6}$$

The second objective aims to improve the surge vibration resistance for constant surge conditions. Of course, in reality surge conditions are not steady-state, since the reversed flow is a shockwave which interrupts the regular flow and stops right after reaching pressure balance between the combustion chamber and the inlet of the engine. However, also a comparison of undamaged and blended objective values for steady conditions can show the right trend of improvement or degradation. Here, the surge *af*-strengths for the six modes in Fig. 16.3 are normalised with respect to the lower bounds used in (16.4), respectively. For minimisation these ratios are inverted and averaged resulting in the objective

$$f_2 = \frac{1}{6}\sum_{i=1}^{6} \frac{af_i^c}{af_{i,\text{surge}}}. \tag{16.7}$$

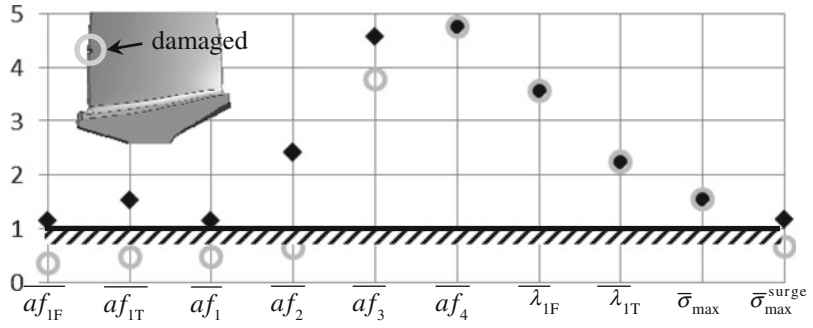

Fig. 16.3 Degradation of normalised endurance measures from undamaged (♦) to damaged (○) blisk aerofoil

Simultaneously, the endurance measures (16.2)–(16.5) have to be fulfilled, which may be summarised in a vector of implicit constraints:

$$\mathbf{h} := \begin{bmatrix} af_j^c/af_j - 1 \\ \sigma_{\max}/R_m - 1 \\ \sigma_{\max}^{\text{surge}}/R_m - 1 \\ \lambda_{1\text{F}}^c/\lambda_{1\text{F}} - 1 \\ \lambda_{1\text{T}}^c/\lambda_{1\text{T}} - 1 \end{bmatrix} \leq \mathbf{0}. \tag{16.8}$$

Finally, a multi-criterion optimisation problem based on (16.1) and (16.6)–(16.8) may be formulated as

$$\min_{\mathbf{p} \in P} \begin{bmatrix} f_1 \\ f_2 \end{bmatrix} \quad \text{where } P = \left\{ \mathbf{p} \in \mathbb{R}^5 | \mathbf{h}(\mathbf{p}) \leq \mathbf{0}, \mathbf{p}^l \leq \mathbf{p} \leq \mathbf{p}^u \right\}. \tag{16.9}$$

Such type of problems may be solved by multi-objective genetic algorithms. However, these algorithms usually require a huge number of design evaluations and a single FE-evaluation already takes about 10–90 min depending on the mesh size at the cutout and hence on the cutout size. Response surface methods help to resolve this problem. They are based on only few evaluated supporting points and are computationally much cheaper than direct FE-analyses. Therefore, the optimisation problem (16.9) is not solved directly, but adaptive, Kriging-based response surfaces are applied which are implemented in the DACE toolbox [9] of MATLAB. Such strategies based on surrogate models are always recommendable in case of computationally expensive problems [4].

A Kriging response surface models a deterministic response function value $f(\mathbf{p})$ as normally distributed random number characterised by mean value $\mu_f(\mathbf{p})$ and standard deviation $s_f(\mathbf{p})$. Then, the most probable realisation of the unknown true function value $f(\mathbf{p})$ is $\mu_f(\mathbf{p})$; however, if minimising $\mu_f(\mathbf{p})$ only, the algorithm may get stuck in a local minimiser. Therefore, the strategy "Minimising a Statistical Lower Bound" [7] is implemented where the artificial objective $\tilde{f}(\mathbf{p}) = \mu_f(\mathbf{p}) - \kappa s_f(\mathbf{p})$, $\kappa \in \mathbb{R}$, is minimised instead. Design points minimising $\tilde{f}(\mathbf{p})$ are worth to be evaluated since they either are points with low function values expressed by low μ_f or high uncertainty expressed by large s_f values. Therefore, the response surface is refined iteratively at these points, where in the following $\kappa = 3$ will be used.

To illustrate this strategy, Fig. 16.4a shows a 1D-example where the unknown original function $f(p)$ is approximated by estimated mean values $\mu_f(p)$ found from a set of supporting points (○). In combination with the predicted standard deviation $s_{f(p)}$, the implemented strategy delivers the goal function $\tilde{f}(p)$ in Fig. 16.4b with minimiser $p*$ which serves as additional supporting point in the next iteration step. This strategy is applied to both objectives f_i resulting in statistical estimates $\mu_{f,i}$, $s_{f,i}$ and constraints h_j resulting in $\mu_{h,j}$, $s_{h,j}$.

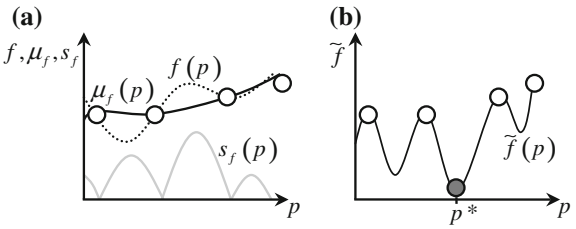

Fig. 16.4 1D-example of Kriging models (**a**) and "Minimising a Statistical Lower Bound" (**b**)

Before solving the optimisation problem (16.9) by the mentioned Kriging strategy, another modification needs to be done to obtain an unconstrained optimisation problem

$$\min_{\mathbf{p} \in P} \begin{bmatrix} \hat{f}_1(\mathbf{p}) \\ \hat{f}_2(\mathbf{p}) \end{bmatrix}. \tag{16.10}$$

Within a penalty strategy, both objectives $\tilde{f}_i(\mathbf{p})$ described above are artificially degraded with the same penalties $w_h(\mathbf{p})$ and $w_{dist}(\mathbf{p})$ as

$$\hat{f}_i(\mathbf{p}) := \mu_{f,i}(\mathbf{p}) - 3s_{f,i}(\mathbf{p}) + (w_h(\mathbf{p}) + w_{dist}(\mathbf{p}))^2 \tag{16.11}$$

where the first penalty term

$$w_h(\mathbf{p}) = \sum_j w_{h,j}(\mathbf{p}),$$
$$w_{h,j}(\mathbf{p}) = \begin{cases} \mu_{h,j}(\mathbf{p}) - 3s_{h,j}(\mathbf{p}) + 1{,}000 & \text{if} \quad \mu_{h,j}(\mathbf{p}) - 3s_{h,j}(\mathbf{p}) > 0 \\ 0 & \text{else} \end{cases} \tag{16.12}$$

deals with constraints (16.8). If the statistical lower bound $\mu_{h,j}(\mathbf{p}) - 3s_{h,j}(\mathbf{p})$ violates the constraint, the real value $h_j(\mathbf{p})$ is unlikely to fulfil it and a high penalty value of 1,000 is added. This value is chosen to guarantee that even feasible designs with poor objective values are rated better than infeasible designs with good objective values.

The second penalty term is intended to avoid designs within the FE-evaluation process where the associated blade cannot be created or analysed. That is why the term $w_{dist}(\mathbf{p})$ in Eq. (16.11) deteriorates the objectives if the distance of a new design suggestion $\mathbf{p}$ is too close to any already known non-converged design $\mathbf{p}_k$ which is stored in an archive:

$$w_{dist}(\mathbf{p}) = \begin{cases} 1{,}000 & \text{if} \quad \min_k |\mathbf{p} - \mathbf{p}_k| \le \varepsilon \\ 0 & \text{else} \end{cases}. \tag{16.13}$$

The unconstrained surrogate optimisation problem (16.10) is solved within the Isight process shown in Fig. 16.5. Firstly, a design of experiments (DoE) defines an initial set of designs which are evaluated by direct analysis. The obtained data

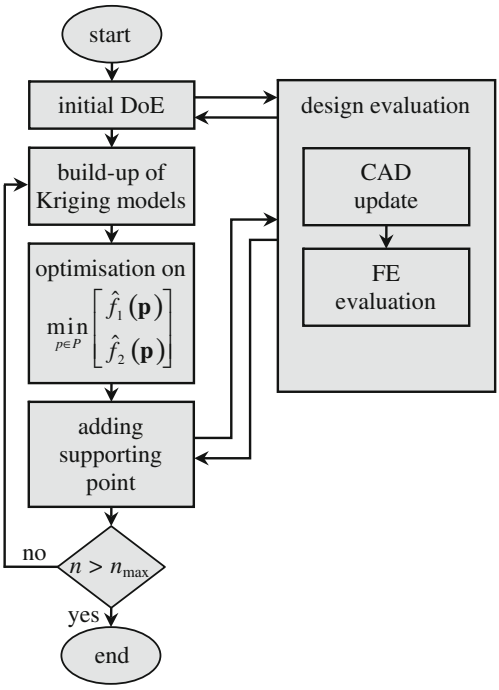

Fig. 16.5 Scheme of optimisation process flow

are used for building up first Kriging models for both criteria (16.6), (16.7) and for the constraints (16.8). Based on these surrogate models a genetic algorithm determines Pareto-optimal solutions in MATLAB for the Kriging-based problem (16.10)–(16.13). The model is then refined iteratively by evaluating and adding the Pareto-optimal solutions with the biggest distance to already converged designs in a user-defined number of loops.

16.4 Optimisation Results

In the following, the settings and the obtained results of the optimisation strategy are described. The initial DoE for creating the first set of Kriging-based surrogate models of objective and constraint functions consists of a Latin hypercube sample of 150 random points. After analysing the function values for these designs, the MATLAB DACE toolbox builds up Kriging models with zero-order polynomial regression models and cubic spline correlation models [9]. The converged points are used as input data whereas non-converged designs cannot contribute since they provide no useful information on objective and constraint functions. The latter points are stored in an archive of non-converged designs to be avoided. The Kriging-based optimisation problem (16.10)–(16.13) is solved by the optimisation algorithm NSGA-II

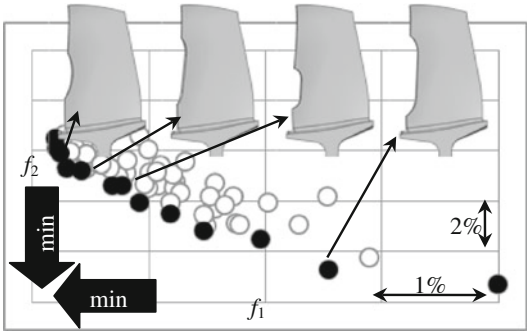

Fig. 16.6 Admissible designs in criterion space (○), Pareto-optimal solutions (●), and examples for optimally blended aerofoil shapes

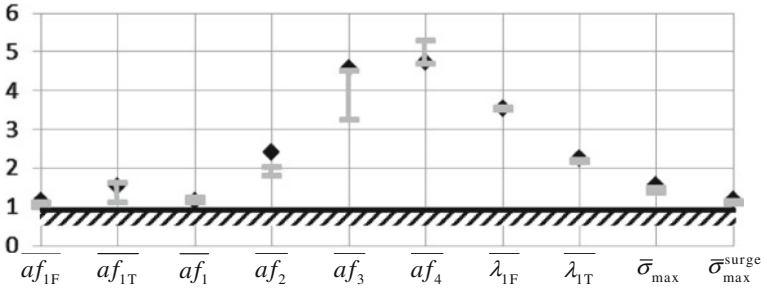

Fig. 16.7 Range of normalised endurance measures for all Pareto-optimal solutions (**I**) compared to the undamaged reference design (♦)

implemented in MATLAB where population size and number of generations are set to 100, respectively. A single solution of the Pareto-optima is chosen such that it has the biggest distance to the already used supporting points. This design point is evaluated according to Fig. 16.5 and used as additional supporting point in the next loop. If it cannot be evaluated, it is assigned to the archive of non-converged designs and the next best Pareto solution is checked. Altogether, 1500 iteration loops are run to update the surrogate models.

The design parameters of the described blending model are limited by confidential geometric bounds $\mathbf{p}^l, \mathbf{p}^u$. The use of these parameter limits and the implemented optimisation strategy are able to recover the endurance measures and result in a wide range of different cutout sizes. Figure 16.6 shows the obtained results in the criterion space defined by original objectives (16.6) and (16.7) as non-dominated solutions and some examples of associated blending shapes. All of the Pareto-optima fulfil the endurance constraints and cope with the initial violation of some endurance measures (Fig. 16.7). From these solutions an engineer may choose a specific blending shape for maintenance repair, where further investigations may be done on aerodynamics to account for the impact on compressor efficiency and surge margin.

Acknowledgments The presented work has been performed within the VIT 3 project (Virtual Turbomachinery) partly funded by the Federal State of Brandenburg, Germany, the European Community, and Rolls-Royce Deutschland. Rolls-Royce Deutschland's permission to publish this work is greatly acknowledged.

References

1. ANSYS Release 13.0 (2010) ANSYS mechanical APDL structural analysis guide. ANSYS Inc., Canonsburg, USA
2. Dassault Systèmes Simulia Corp. (2009) Isight 4.0 component guide. Engineous software Inc., Cary
3. Day WD, Fiebiger SW, Patel HN (2012) Parametric evaluation of compressor blade blending, GT2012-68641. In: Proceedings of ASME turbo expo, Copenhagen
4. Giannakoglou KC, Karakasis MK, Kampolis IC (2006) Evolutionary algorithms with surrogate modeling for computationally expensive optimization problems. In: Proceedings ERCOFTAC, Gran Canaria, Spain
5. Gietl T (2012) HPC blade borescope blend repair limits-aerodynamic assessment. Technical Report, Rolls-Royce Deutschland, Dahlewitz
6. Hoenick M (2009) Blisk blending repair-stress assessment. Technical Report, Rolls-Royce Deutschland, Dahlewitz
7. Jones DR (2001) A taxonomy of global optimization methods based on response surfaces. J Glob Optim 21:345–383
8. Karger K, Bestle D (2012) Multi-objective blisk optimisation taking into account environmental influences. In: Proceedings of the 5th IC-SCCE, Athens
9. Lophaven SN, Nielsen HB, Søndergaard J (2002) DACE—A MATLAB Kriging toolbox, Informatics and mathematical modelling, Technical University of Denmark
10. Otto D (2009) Ein Beitrag zur interdisziplinären Prozessintegration und automatischen Mehrzieloptimierung am Beispiel einer Verdichterrotorschaufel. Dissertation, Shaker-Verlag, Aachen
11. Pianka C (2009) MMM21300: Mechanical assessments and criteria for compressor blisk designs regarding the aerofoil integrity. Technical Report, Rolls-Royce Deutschland, Dahlewitz
12. Wuthe F, Pianka C (2012) HPC gaspath boroscope examination. Technical Report, Rolls-Royce Deutschland, Dahlewitz